PHOTONICS Research

Revealing the dynamics of intensity fluctuation transfer in a random Raman fiber laser

Jun Ye,[1] Xiaoya Ma,[1] Yang Zhang,[1] Jiangming Xu,[1,2] Hanwei Zhang,[1] Tianfu Yao,[1] Jinyong Leng,[1] and Pu Zhou[1,3]

[1]College of Advanced Interdisciplinary Studies, National University of Defense Technology, Changsha 410073, China
[2]e-mail: jmxu1988@163.com
[3]e-mail: zhoupu203@163.com

Received 12 October 2021; revised 28 December 2021; accepted 29 December 2021; posted 4 January 2022 (Doc. ID 445432); published 9 February 2022

Temporal intensity fluctuation is one of the inherent features of fiber lasers. When utilizing the fiber lasers to pump a random Raman fiber laser (RRFL), the intensity fluctuation transfer from the pump to the random lasing could affect the output performance significantly. In this paper, we comprehensively compared the spectral, temporal, and power characteristics of an RRFL pumped by two different fiber lasers—a temporally unstable fiber oscillator and a temporally stable amplified spontaneous emission (ASE) source. Owing to less impact of the intensity fluctuation transfer, the ASE source-pumped RRFL shows ~45.3% higher maximum output power, higher spectral purity (>99.9%) and optical signal-to-noise ratio (>40 dB), weaker spectral broadening, and more stable temporal behavior compared to the fiber oscillator-pumped RRFL. Furthermore, based on the temporal-spatial-coupled Raman equations and the generalized nonlinear Schrödinger equations, we numerically revealed the impact of the pump intensity fluctuations on the output characteristics of RRFLs, and found that the temporal walk-off effect played an important role in the dynamics of intensity fluctuation transfer. This work may provide a reference for designing and implementing high-performance RRFLs and promote their practicability in sensing, telecommunications, and high-power applications.

https://doi.org/10.1364/PRJ.445432

1. INTRODUCTION

By employing Rayleigh backscattering in long passive fibers to provide random distributed feedback (RDFB), random Raman fiber lasers (RRFLs) can operate without point-based reflectors and are easy to implement [1,2]. As a new branch of Raman fiber lasers (RFLs), RRFLs have inherited the merits such as wavelength flexibility, high power scalability, and excellent beam quality [3,4]. Besides, the RDFB mechanism brings about the mode-free characteristic [5] and distinctive statistical properties [6–8], which makes the RRFLs quite interesting and excellent platforms for scientific research and practical application [9–13].

Since the first demonstration in 2010 [1], RRFLs have attracted widespread attention [2,12,13], and obtaining high-performance RRFLs has always been researchers' goal and aspiration. The passive fiber and the pump source are two key components that can be optimized to improve the laser performance. For example, to realize high-power RRFLs, the passive fiber is optimized to be shorter [14], with a larger core and a lower numerical aperture (NA), to suppress high-order stimulated Raman scattering (SRS) and four-wave mixing assisted SRS effect [15,16]. In order to obtain special operating wavelengths with fewer orders of Raman conversion, the commonly used telecom fibers are replaced by phosphosilicate fibers, which have a Raman gain peak at the frequency shift of ~39.8 THz (about 3 times as high as that of the telecom fibers) [17,18]. Most of the previously reported RRFLs are pumped by rear-earth-doped fiber oscillators or Raman fiber oscillators [19,20]; although relative intensity-noise (RIN) transfer in RRFLs was studied as early as 2012 [21], our approach combines for the first time experiment and full modeling to offer a complete picture of the role of these fluctuations on the output characteristics of an RRFL.

Recent investigations have proven that the temporal characteristics of pump sources can be transmitted to RRFLs; the optimization of pump sources is therefore deemed necessary [22,23]. The amplified spontaneous emission (ASE) source, which has higher temporal stability than fiber oscillators, began to be used as the pump source [24–28]. The high temporal stability of the ASE source has significantly improved the output performance of RRFLs, particularly the spectral purity of generated random lasing. For example, with the pumping of the 1 μm ASE source, the maximum spectral purity of the 1st-order Stokes wave can even exceed 99.9% [26], and that

of the 8th-order Stokes wave at 1.7 μm can also reach as high as ~98.3% [27]. Incidentally, the pumping of the ASE source has not only improved the output performance of RRFLs but also benefited conventional RFLs [29] and Raman fiber amplifiers [30,31]. Indeed, the transfer of pump intensity fluctuations in Raman fiber amplifiers [32,33] and supercontinuum sources [34,35] has been well explored, in which the dispersive walk-off effect and the nonlinear effects such as cross-phase modulation (XPM) and modulation instability play important roles in the dynamics. In RRFLs, however, the impact of the pump source on the output characteristics has not been comprehensively clarified, especially the influence of the intensity fluctuation transfer. Besides, the underlying dynamics have not been revealed in theoretical simulations.

In this paper, with the pumping of two different fiber lasers—a temporally unstable fiber oscillator and a temporally stable ASE source, we experimentally compared the spectral, temporal, and power characteristics of an RRFL in detail. Based on the temporal-spatial-coupled cascaded Raman equations, we numerically investigated the transfer of the pump intensity fluctuations as a function of fluctuation amplitude and frequency. We also analyzed the influences of the walk-off parameter and fiber length on the intensity fluctuation transfer. Furthermore, using the generalized nonlinear Schrödinger equations (GNLSEs), we simulated the temporal, spectral, and power characteristics of an RRFL pumped by an ASE source and a fiber oscillator. We believe this work can help understand the impact of pump intensity fluctuations on the output characteristics of RRFLs and provide a reference for the design and implementation of high-performance RRFLs.

2. EXPERIMENTAL SETUP

The experimental setup is described in Fig. 1(a). The RRFL has a forward-pumped half-open cavity, in which a narrowband ASE source and a fiber oscillator are employed as the pump source separately. The ASE source and the fiber oscillator operate at ~1067.4 nm, and the maximal output powers reach more than 20 W. The pump light is injected through the signal port (1070 nm) of a wavelength division multiplexer (WDM), and the tap port (1120 nm) of the WDM is spliced with a fiber Bragg grating (FBG) operating at 1120 nm. The FBG has a reflectivity of 55% and a 3-dB reflection bandwidth of 0.4 nm. Considering the splice loss and the insertion loss of the WDM, the effective reflectivity of the FBG is estimated to be 40%. The common port of the WDM is followed by a 2-km-long G.652.D passive fiber, which features a core diameter of 8.2 μm, a cladding diameter of 125 μm, and a numerical aperture (NA) of 0.14. In addition, all the end facets are cleaved at an angle of 8° to suppress undesired reflection.

Figure 1(b) displays the temporal profiles of the fiber oscillator and the ASE source at their maximum output powers. The measurement unit includes a photodetector (5 GHz bandwidth, rise time <70 ps) and an oscilloscope (1 GHz bandwidth, 5 GS/s sampling rate). The mean value of temporal intensities is normalized to 1 for ease of comparison. Apparently, the fiber oscillator has stronger temporal fluctuations than the ASE source. The normalized standard deviation (STD) and peak-to-valley (P-V) value of the temporal fluctuations of the fiber oscillator are 5.2% and 41.8%, respectively. In comparison, the corresponding values of the ASE source are

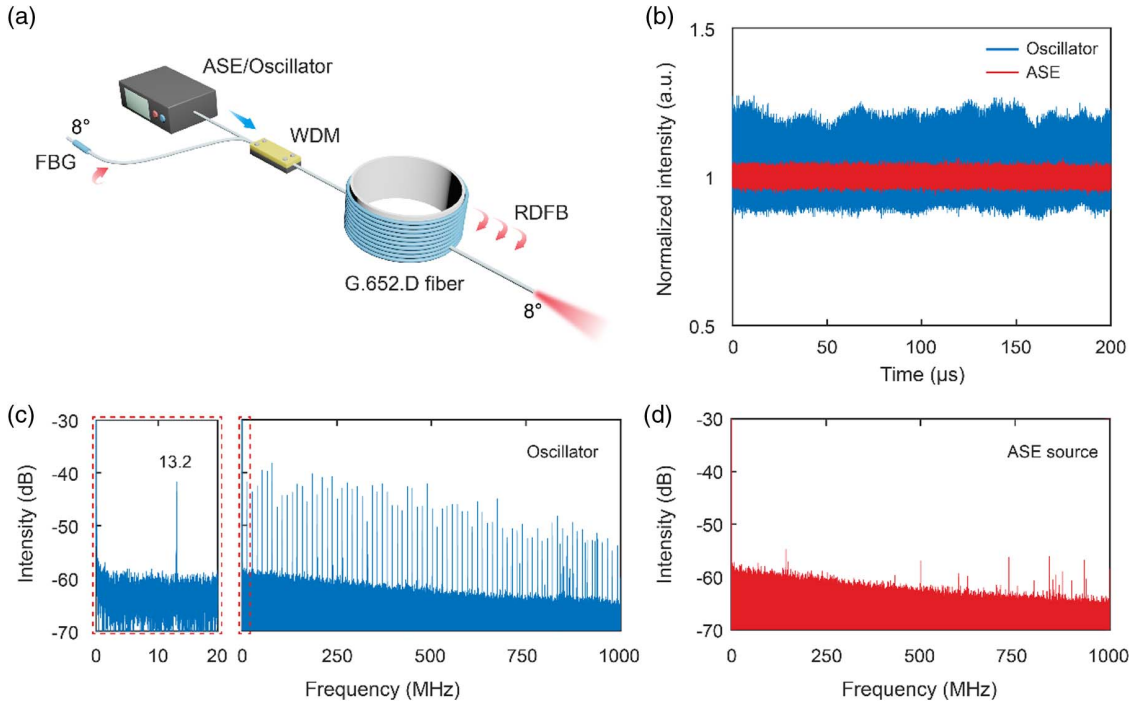

Fig. 1. (a) Schematic of the experimental setup. ASE, amplified spontaneous emission; WDM, wavelength division multiplexer; FBG, fiber Bragg grating; RDFB, random distributed feedback. (b) Normalized temporal profiles of the fiber oscillator and the ASE source. Radio frequency (RF) spectra of (c) the fiber oscillator and (d) the ASE source. Inset of (c) shows a zoom-in around the fundamental repetition rate of the fiber oscillator.

only 1.3% and 12.9%. The radio frequency (RF) spectrum of the fiber oscillator is presented in Fig. 1(c), which shows a fundamental repetition rate of 13.2 MHz (see the inset), and a comb of the harmonic frequencies over the whole range of 1 GHz. The fundamental repetition rate exactly corresponds to the cavity length of the fiber oscillator, indicating that there are self-mode locking pulses in the temporal behavior [36]. Figure 1(d) shows the RF spectrum of the ASE source, which has no characteristic frequency except for some environmental noises.

3. EXPERIMENTAL RESULTS

A. Spectral Characteristics of the RRFL

The spectral evolutions of the RRFL pumped by the fiber oscillator and the ASE source are, respectively, shown in Figs. 2(a) and 2(b). The three insets at the bottom present the output spectrum below the threshold, near the threshold, and well above the threshold, while the two insets at the top, respectively, display the output spectrum at the maximum output power and well above the 2nd-order threshold. There is a big difference in the output spectra near the threshold. The fiber oscillator-pumped RRFL shows a narrow and weak peak at 1120 nm, while the ASE source-pumped counterpart has a very spiky output spectrum; even the 2nd-order Stokes wave can be observed. With the further increase of pump power, the spiky output spectrum gradually becomes stabilized and the 2nd-order Stokes wave disappears. This phenomenon could be attributed to the cascaded stimulated Brillouin scattering (SBS) process [1,37].

The maximum optical signal-to-noise ratio (OSNR, the intensity difference between the 1st-order Stokes wave and the residual pump light) also differs greatly. As shown in Fig. 2(c), with the pumping of the fiber oscillator, the maximum OSNR of the output spectrum is ~20.9 dB, while with the pumping of the ASE source, the maximum OSNR reaches as high as ~40.8 dB. Different pumping also has an impact on the spectral purity (power-in-band ratio) of generated random lasing. For example, the maximum spectral purity with the pumping of the fiber oscillator is ~98.7%, while that with the pumping of the ASE source exceeds 99.9%. Furthermore, there are also some differences in linewidth evolution. Figures 2(d) and 2(e), respectively, illustrate the full width at half-maximum (FWHM) linewidth and 10-dB linewidth as functions of pump power. Owing to the cascaded SBS effect, the RRFL pumped by the ASE source shows a relatively broad spectrum near the threshold. The FWHM linewidth and the 10-dB linewidth, respectively, reach 0.39 and 3.72 nm with 4.9 W pump power. With the increase of the pump power, the output spectrum becomes stabilized and the linewidth narrows. With the pump power higher than 6.5 W, the spectral linewidth gradually broadens. In comparison, the output spectrum of the fiber-oscillator-pumped RRFL shows a monotonic broadening. Besides, the spectral broadening with the pumping of the fiber oscillator is stronger, and the spectral linewidths are broader with the same pump power. The spectral evolutions show that

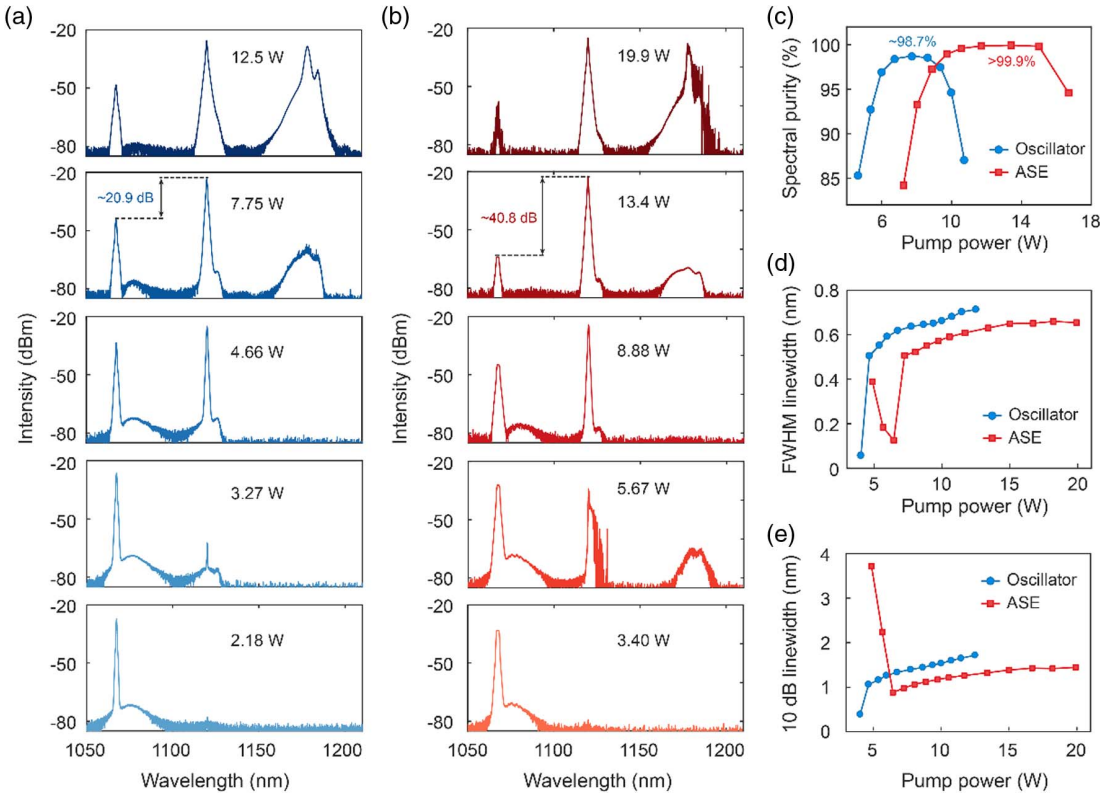

Fig. 2. Spectral evolution of the RRFL pumped by (a) the fiber oscillator and (b) the ASE source. Legends indicate the injected pump powers. (c) Spectral purity, (d) FWHM linewidth, and (e) 10-dB linewidth of the 1st-order Stokes wave as functions of pump power.

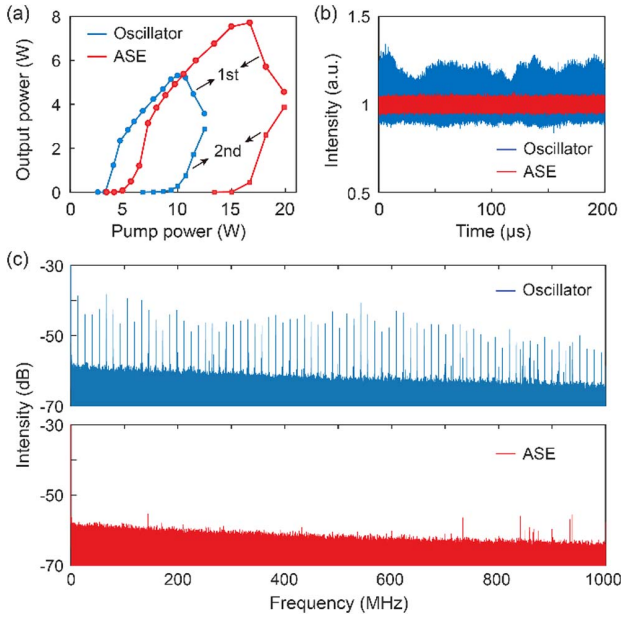

Fig. 3. (a) Output powers of the 1st-order Stokes wave (circles) and the 2nd-order Stokes wave (squares). (b) Temporal profiles and (c) corresponding RF spectra of the 1st-order Stokes wave at the maximum output powers. Blue lines (points) and red lines (points), respectively, indicate the results pumped by the fiber oscillator and ASE source.

a temporally stable pump source can improve the maximum OSNR and spectral purity and suppress the spectral broadening of RRFLs.

B. Temporal and Power Characteristics of the RRFL

We also compared the temporal and power characteristics of the RRFL. Figure 3(a) displays the power evolutions of the 1st- and 2nd-order Stokes waves. The threshold pump power with the pumping of the fiber oscillator is ~3.3 W, while that with the pumping of the ASE source increases to ~4.9 W. The maximum output power of the fiber-oscillator-pumped RRFL is ~5.3 W, while the ASE-source-pumped RRFL shows a maximum power of ~7.7 W, which is ~45.3% higher than that pumped by the fiber oscillator. The power evolution indicates that a temporally stable pump source can suppress the high-order SRS effect and significantly improve the maximum output power of RRFLs.

The temporal profiles of the 1st-order Stokes wave with the maximum output powers are plotted in Fig. 3(b). Obviously, the temporal fluctuations of the fiber-oscillator-pumped RRFL are much stronger; the normalized STD and the P-V value of intensity fluctuations are 4.9% and 50.5%, respectively. In comparison, the corresponding values with the pumping of the ASE source decrease to 1.5% and 14.4%. The contrast in the temporal profiles indicates that the temporal fluctuations have been transferred from the pump source to the RRFL [22,24]. The RF spectra can further prove this conclusion, as presented in Fig. 3(c). The RF spectrum of generated random lasing is nearly identical to that of the pump source [see Figs. 1(c) and 1(d)]. The self-mode locking characteristic of the fiber oscillator has transmitted to the RRFL, which explains the strong temporal fluctuations of the generated random lasing in that case.

4. THEORETICAL ANALYSIS

A. Role of Fluctuation Amplitude and Temporal Walk-off Effect

The experimental results described above have shown the impact of pump intensity fluctuations on the output performance of RRFLs. However, the underlying physical mechanism has not been revealed. The transfer of pump intensity fluctuations seems critical, but the affecting factors have not been figured out. Therefore, we first carried out the simulation based on the temporal-spatial-coupled cascaded Raman equations and tried to qualitatively explain the role of fluctuation amplitude, frequency, and the temporal walk-off effect.

For a forward-pumped RRFL, the temporal-spatial-coupled cascaded Raman equations can be written as [5,38]

$$\frac{\mathrm{d}P_0^+}{\mathrm{d}z}+\frac{1}{v_{g0}}\frac{\mathrm{d}P_0^+}{\mathrm{d}t}=-\alpha_0 P_0^+-\frac{\lambda_1}{\lambda_0}g_{R1}(P_1^++P_1^-+4h\nu_1\Delta\nu_1B_1)P_0^+, \tag{1}$$

$$\frac{\mathrm{d}P_1^\pm}{\mathrm{d}z}\pm\frac{1}{v_{g1}}\frac{\mathrm{d}P_1^\pm}{\mathrm{d}t}=\pm g_{R1}P_0^+(P_1^\pm+2h\nu_1\Delta\nu_1B_1)\pm\varepsilon_1P_1^\mp \mp\frac{\lambda_2}{\lambda_1}g_{R2}(P_2^++P_2^-+4h\nu_2\Delta\nu_2B_2)P_1^\pm\mp\alpha_1P_1^\pm, \tag{2}$$

$$\frac{\mathrm{d}P_2^\pm}{\mathrm{d}z}\pm\frac{1}{v_{g2}}\frac{\mathrm{d}P_2^\pm}{\mathrm{d}t}=\pm g_{R2}(P_1^++P_1^-)(P_2^\pm+2h\nu_2\Delta\nu_2B_2)\pm\varepsilon_2P_2^\mp\mp\alpha_2P_2^\pm, \tag{3}$$

$$B_j=1+\frac{1}{\exp\left[\frac{h(\nu_{j-1}-\nu_j)}{k_BT}\right]-1}\qquad(j=1,2), \tag{4}$$

where the subscripts 0, 1, and 2, respectively, denote the pump wave, the 1st-order Stokes wave, and the 2nd-order Stokes wave. P represents the power as a function of time t and position z. The superscripts + and – stand for the forward and backward direction, respectively. v_g denotes the group velocity in the fiber core. α is the attenuation coefficient, and ε is the Rayleigh backscattering coefficient. λ stands for the optical wavelength, ν is the wave frequency, and $\Delta\nu$ is the effective bandwidth. g_R represents the Raman gain coefficient. B is the population of photons which introduce the noise from spontaneous Raman scattering. In addition, h is the Planck constant, k_B is the Boltzmann constant, and T represents the fiber temperature.

The boundary conditions are given by

$$P_0^+(z=0,t)=P_{\mathrm{in}}(t), \tag{5}$$

$$P_{1,2}^+(z=0,t)=R_{L1,2}P_{1,2}^-(z=0,t), \tag{6}$$

$$P_{1,2}^-(z=L,t)=R_{R1,2}P_{1,2}^+(z=L,t), \tag{7}$$

Table 1. Parameter Values in the Simulation (Part I)

Parameter	Symbol	Value
Attenuation coefficient	$\alpha_0, \alpha_1, \alpha_2$	3.00×10^{-4} m^{-1}, 2.94×10^{-4} m^{-1}, 2.88×10^{-4} m^{-1}
Bandwidth	$\Delta\nu_1, \Delta\nu_2$	0.25 THz
Wavelength	$\lambda_0, \lambda_1, \lambda_2$	1067, 1120, 1178 nm
Left reflectivity	R_{L1}, R_{L2}	$0.4 \times 10^{-5}, 4 \times 10^{-5}$
Right reflectivity	R_{R1}, R_{R2}	4×10^{-5}
Group velocity	v_{g0}, v_{g1}, v_{g2}	2.0421×10^8 m/s, 2.0427×10^8 m/s, 2.0432×10^8 m/s
Raman gain coefficient	g_{R1}, g_{R2}	0.64, 0.61 W^{-1}/km
Rayleigh backscattering coefficient	$\varepsilon_0, \varepsilon_1, \varepsilon_2$	0.51×10^{-6} m^{-1}, 0.50×10^{-6} m^{-1}, 0.49×10^{-6} m^{-1}

where P_{in} represents the input pump power, L is the fiber length, and $R_{L1,2}$ and $R_{R1,2}$ stand for the reflectivity of the left and the right end, respectively. The parameter values used in the numerical simulations are listed in Table 1.

To investigate the impact of the pump fluctuation amplitude and frequency on the intensity fluctuation transfer, we have simplified the input pump power as a sine function of time t. We hope this method can provide a qualitative view of the underlying physical mechanism. Under this simplification, the input power can be written as [39]

$$P_{\text{in}}(t) = P_{\text{avg}} + A_f \sin(2\pi f t - \pi/2), \quad (8)$$

where P_{avg} denotes the average pump power, A_f stands for the fluctuation amplitude, and f represents the fluctuation frequency. Figures 4(a) and 4(b) show the longitudinal power distributions with different pump fluctuation amplitudes. The average pump power P_{avg} is fixed at 15 W, and the fluctuation frequency is assumed to be 10 MHz. The fluctuation amplitude for Figs. 4(a) and 4(b) is set to 2 and 5 W, respectively. The snapshot of the longitudinal power distributions proves that the temporal fluctuation characteristic has been transferred from the pump source to the RRFL. With the pump fluctuation amplitude of 2 W [Fig. 4(a)], the average output power of the 1st-order Stokes wave reaches 7.76 W, with a fluctuation amplitude of 0.98 W. The residual pump power and the 2nd-order Stokes power are close to 0. In comparison, when the pump fluctuation amplitude increases to 5 W [Fig. 4(b)], the average output power of the 1st-order Stokes wave drops down to 6.95 W, but the fluctuation amplitude increases to 1.97 W. Moreover, the 2nd-order Stokes wave grows significantly near the fiber end; its average output power reaches 0.67 W. Additionally, the residual pump power is still close to 0, but it is ~7 times that with the pump fluctuation amplitude of 2 W.

Figure 4(c) illustrates the temporal fluctuation amplitude of the 1st-order Stokes wave versus that of the pump wave. For ease of comparison, we introduce the normalized fluctuation amplitude (NFA), which is defined as A_f/P_{avg}. The NFA of the generated random lasing monotonically increases with that of the pump source, indicating that a temporally unstable

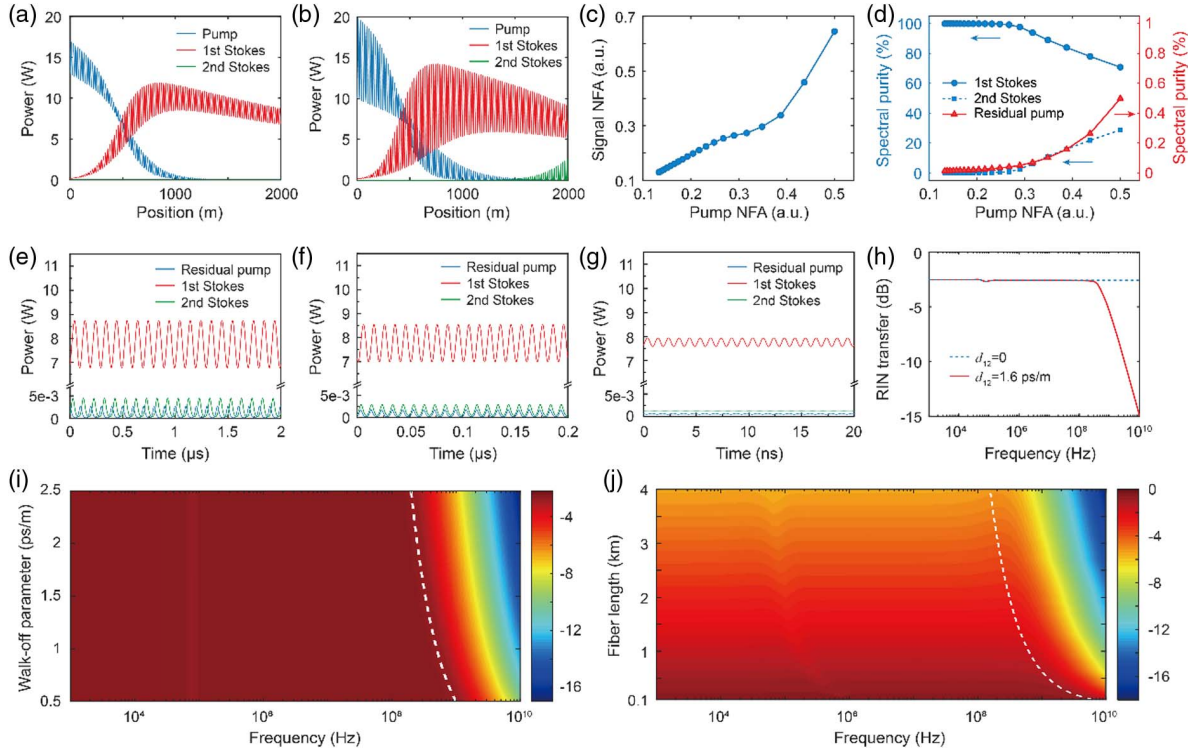

Fig. 4. Snapshot of longitudinal power distributions with the pump fluctuation amplitude of (a) 2 W and (b) 5 W. (c) Normalized fluctuation amplitude (NFA) of the 1st-order Stokes wave as a function of the pump NFA. (d) Spectral purity dependence on the pump NFA. Note that the pump fluctuation frequency for (a)–(d) is fixed at 10 MHz. Output temporal behaviors with different pump fluctuation frequencies of (e) 10 MHz, (f) 100 MHz, and (g) 1 GHz. (h) RIN transfer with and without temporal walk-off effect. The total pump power is 10 W, and the fiber length is 2 km. RIN transfer dependence on (i) walk-off parameter and (f) fiber length.

pump source could generate a temporally unstable RRFL. We also investigate the effect of pump fluctuation amplitude on the spectral purities (power-in-band ratios). As shown in Fig. 4(d), when the pump source's NFA increases from 0.13 to 0.25, the spectral purity of the 1st-order Stokes wave drops from 99.96% to 99.65%, and the proportions of the residual pump wave and the 2nd-order Stokes wave show only a slight increase. However, when the pump source's NFA further increases from 0.25 to 0.5, the spectral purity of the 1st-order Stokes wave decreases linearly to ~70.8%, while the proportions of the residual pump wave and the 2nd-order Stokes wave, respectively, increase to ~0.5% and ~28.7%. The above results manifest that under the same average pump power, a stronger pump intensity fluctuation could degrade the spectral purity of the desired random lasing (the 1st-order Stokes wave), resulting in more residual pump power and the early onset of the 2nd-order Stokes wave.

The above simulations are under the pump fluctuation frequency of 10 MHz, so another question is how the pump fluctuation frequency influences the output performance of RRFL. Figures 4(e), 4(f), and 4(g) plot the output temporal behaviors with different pump fluctuation frequencies of 10 MHz, 100 MHz, and 1 GHz, respectively. The average input pump power is 15 W, and the pump fluctuation amplitude is fixed at 2 W. When the pump fluctuation frequency increases from 10 to 100 MHz, the average output power of the 1st-order Stokes wave was almost unchanged, but the fluctuation amplitude slightly drops from 0.98 to 0.78 W. When the pump fluctuation frequency further increases to 1 GHz, the fluctuation amplitude of the 1st-order Stokes wave shows a significant decrease to 0.18 W, indicating that the transfer of the pump intensity fluctuations weakens sharply at a certain frequency [21,40]. In other words, there exists a cut-off frequency for the transfer of the pump intensity fluctuations.

The transfer of the pump intensity fluctuations weakened at high frequencies could be attributed to the temporal walk-off effect. This effect occurs due to the mismatch of group velocities [41]. Here we introduce the walk-off parameter d_{01}, which is defined as $1/v_{g0} - 1/v_{g1}$. For the pump wave at 1067.4 nm and the 1st-order Stokes wave at 1120 nm, the walk-off parameter is ~1.6 ps/m, meaning that the temporal walk-off between the pump wave and the 1st-order Stokes wave reaches 1.6 ps with 1-m-long propagation. To further figure out the role of the fluctuation frequency on the transfer of the pump intensity fluctuations, we numerically calculated the RIN transfer function [40]. As shown in Fig. 4(h), the cut-off frequency is located near 300 MHz (red line), which agrees well with the approximation $1/(d_{01} \times L) = 312.5$ MHz. In comparison, if we neglect the temporal walk-off effect, there will be no cut-off frequency (blue-dashed line). So we can conclude that the RRFLs are mainly influenced by the pump intensity fluctuations' low-frequency components (lower than the cut-off frequency), and the cut-off frequency is determined by the temporal walk-off effect.

The question further becomes, what could influence the temporal walk-off effect. Apparently, it is the walk-off parameter and fiber length. Figure 4(i) presents the RIN transfer dependence on the walk-off parameter; note that the fiber length is fixed at 2 km. When the walk-off parameter increases from 0.5 to 2.5 ps/m, the cut-off frequency decreases from 1 GHz to 200 MHz. Besides, the cut-off frequency dependence on the walk-off parameter can also be well approximated by $1/(d_{01} \times L)$ (the white-dashed line). This result means that the higher the walk-off parameter, the lower the cut-off frequency, and the less impact of pump intensity fluctuations on the RRFL. This conclusion is quite beneficial to large-frequency-shift RRFLs [17,18]. For example, for the phosphosilicate RRFL using a 1064-nm pump wave to generate a 1240-nm signal wave, the walk-off parameter reaches 3.3 ps/m. Thus, the corresponding cut-off frequency will decrease to ~150 MHz, indicating that the large-frequency-shift RRFL has an excellent filtering effect on the pump intensity fluctuations.

Figure 4(j) shows the RIN transfer dependence on the fiber length, in which the walk-off parameter is fixed at 1.6 ps/m. It is seen that a longer fiber length will result in a lower cut-off frequency, meaning that the longer-cavity RRFLs have a better filtering effect on the pump intensity fluctuations. However, the approximation of cut-off frequency $1/(d_{01} \times L)$ (the white-dashed line) does not agree well with the numerical simulations with relatively long fiber lengths, since the random lasing is always generated at the posterior segment of the passive fiber and the effective length will be shorter than the total fiber length. It is worth noting that in very long fibers, the effective length is determined by the attenuation coefficient [2]; thus, further increasing the fiber length will have little impact on the cut-off frequency. Furthermore, for high-power RRFLs, the fiber lengths are very small, and the cut-off frequency even reaches the 10 GHz level for a 100-m-long fiber length. This result indicates that the pump intensity fluctuations will significantly influence the high-power short-cavity RRFLs. A temporally stable pump source is extremely important to high-power, high-spectral-purity RRFLs.

B. Simulations Based on GNLSEs

The above simulations have provided a qualitative view of the impact of the pump intensity fluctuations on RRFLs. However, one cannot obtain the spectral and temporal characteristics of the RRFLs with different pump sources, as the cascaded Raman equations concern only the power evolutions. In this section, we further numerically investigated the spectral and temporal characteristics of the RRFL using the GNLSEs.

Neglecting the interaction between the pump wave and the 2nd-order Stokes wave, the GNLSEs for a forward-pumped RRFL can be written as [6,41]

$$\frac{\partial A_0}{\partial z} = -d_{01}\frac{\partial A_0}{\partial t} - \frac{i}{2}\beta_{2p}\frac{\partial^2 A_0}{\partial t^2} + i\gamma_0[|A_0|^2 + (2-f_R)|A_1^+|^2]A_0 - \frac{\alpha_0}{2}A_p - \frac{g_{R1}\lambda_1}{2\lambda_0}(|A_1^+|^2 + \langle|A_1^-|^2\rangle)A_0, \tag{9}$$

$$\frac{\partial A_1^+}{\partial z} = -\frac{i}{2}\beta_{2s}\frac{\partial^2 A_1^+}{\partial t^2} + i\gamma_1[|A_1^+|^2 + (2-f_R)(|A_0|^2 + |A_2^+|^2)]A_1^+ - \frac{\alpha_1}{2}A_1^+ + \frac{g_{R1}}{2}|A_0|^2 A_1^+ + \frac{\varepsilon_1}{2}A_1^- - \frac{g_{R2}\lambda_2}{2\lambda_1}(|A_2^+|^2 + \langle|A_2^-|^2\rangle)A_1^+, \tag{10}$$

$$\frac{\partial A_1^-}{\partial z} = -\frac{i}{2}\beta_{2s}\frac{\partial^2 A_1^-}{\partial t^2} + i\gamma_1[|A_1^-|^2 + (2-f_R)|A_2^-|^2]A_1^- - \frac{\alpha_1}{2}A_1^- + \frac{g_{R1}}{2}\langle|A_0|^2\rangle A_1^- + \frac{\varepsilon_1}{2}A_1^+ - \frac{g_{R2}\lambda_2}{2\lambda_1}(|A_2^-|^2 + \langle|A_2^+|^2\rangle)A_1^-, \tag{11}$$

$$\frac{\partial A_2^+}{\partial z} = -\frac{i}{2}\beta_{2b}\frac{\partial^2 A_2^+}{\partial t^2} + i\gamma_2[|A_2^+|^2 + (2-f_R)|A_1^+|^2]A_2^+ - \frac{\alpha_2}{2}A_2^+ + \frac{\varepsilon_2}{2}A_2^- + d_{12}\frac{\partial A_2^+}{\partial t} + \frac{g_{R2}}{2}(|A_1^+|^2 + \langle|A_1^-|^2\rangle)A_2^+, \tag{12}$$

$$\frac{\partial A_2^-}{\partial z} = -\frac{i}{2}\beta_{2b}\frac{\partial^2 A_2^-}{\partial t^2} + i\gamma_2[|A_2^-|^2 + (2-f_R)|A_1^-|^2]A_2^- - \frac{\alpha_2}{2}A_2^- + \frac{\varepsilon_2}{2}A_2^+ + d_{12}\frac{\partial A_2^-}{\partial t} + \frac{g_{R2}}{2}(|A_1^-|^2 + \langle|A_1^+|^2\rangle)A_2^-, \tag{13}$$

where A is the optical field envelope, β_{2p}, β_{2s}, and β_{2b}, respectively, denote the 2nd-order dispersion coefficient of the pump wave, the 1st-order Stokes wave, and the 2nd-order Stokes wave. γ stands for the Kerr nonlinearity coefficient. f_R represents the fractional contribution of the delayed Raman response, which is estimated to be 0.18. Other symbols have the same meanings as those in the previous section. The boundary conditions have the following form:

$$A_0(0,t) = A_{\text{in}}, \tag{14}$$

$$\tilde{A}_{1,2}^+(0,\omega) = \sqrt{R_{L1,2}(\omega)}\tilde{A}_{1,2}^-(0,\omega), \tag{15}$$

$$\tilde{A}_{1,2}^-(L,\omega) = \sqrt{R_{R1,2}(\omega)}\tilde{A}_{1,2}^+(L,\omega), \tag{16}$$

where $\tilde{A}(z,\omega)$ represents the complex field in the frequency domain. $R(\omega)$ is the reflective spectrum of the cavity end.

To simulate the influence of the pump intensity fluctuations on the output performance of RRFLs, it is critical to model the input pump waves. The most promising model is to simulate the actual laser oscillation using the set of coupled NLSEs and rate equations. However, this method is extremely time-consuming and is sensitive to boundary conditions [42,43]. Therefore, here we treat the input pump wave as a sum of Fourier components [44]:

$$A_{\text{in}} = \sum_m \hat{X}_m \exp(im\Delta\omega t), \tag{17}$$

where the Fourier modes $\hat{X}_m = |\hat{X}_m|\exp[i\varphi_1(\omega_m)]$ are complex variables, and the phases φ_1 are considered as partially correlated [45]:

$$\varphi_1(\omega_m) = (1-q)\times\varphi_0(\omega_m) + q\times\varphi_1(\omega_{m-1}), \tag{18}$$

in which q is the correlation coefficient, and φ_0 is the random phase uniformly distributed between 0 and 2π. In addition, the power spectrum of the pump field is assumed to be Gaussian with an FWHM linewidth of Ω_L [46]:

$$|\tilde{A}_{\text{in}}(\omega)|^2 = n_0 \exp\left[-4\ln(2)\frac{\omega^2}{\Omega_L^2}\right]. \tag{19}$$

The new parameters' values are provided in Table 2. In addition, the correlation coefficient q for the ASE source and the fiber oscillator is set to 0 and 0.12, respectively [47].

Table 2. Parameter Values in the Simulation (Part II)

Parameter	Symbol	Value
2nd-order dispersion coefficient	$\beta_{2p}, \beta_{2s}, \beta_{2b}$	19.3, 15.1, 10.7 ps^2/km
Kerr nonlinearity coefficient	$\gamma_0, \gamma_1, \gamma_2$	2.39, 2.28, 2.17 W^{-1}/km
Walk-off parameter	d_{01}, d_{12}	1.60, 1.08 ps/m

The spectral FWHM linewidth of the fiber oscillator is 0.4 nm, while that of the ASE source is 2 nm. More importantly, the effective Raman gain coefficients are dependent on the pump fluctuation amplitude [see Figs. 4(a) and 4(b)]. The effective Raman gain coefficient with the pumping of a temporally unstable source seems much higher. In our case, the effective Raman gain coefficients g_{R1} and g_{R2} with the pumping of the fiber oscillator are estimated to be 1.05 and 0.89 W^{-1}/km through fitting the experimental power evolutions.

Figure 5(a) plots the simulated power evolutions with the pumping of the fiber oscillator and ASE source. As can be seen, compared to the fiber-oscillator-pumped RRFL, the 1st-order threshold of the ASE-source-pumped RRFL is 69% higher, the 2nd-order threshold is 56% higher, and the maximum power of the 1st-order Stokes wave is 43% higher. Therefore, a temporally stable pump source is of great value to high-power RRFLs. By fixing the pump power at 8 W, we compared the longitudinal power distributions for the pumping of the fiber oscillator and ASE source. As shown in Fig. 5(b), the power distribution differs greatly. Owing to the higher effective Raman gain coefficient caused by strong pump intensity fluctuations, the 1st-order Stokes wave with the fiber oscillator pumping grows faster, and the power reaches the maximum at ~1200 m. While with ASE source pumping, the 1st-order Stokes wave grows to the maximum at the fiber end.

The simulated optical spectra of the 1st-order Stokes wave are shown in Fig. 5(c), and the experimental output spectra are provided in Fig. 5(d) for comparison. The simulated output spectra agree well with the experimental results. With the same pump power of 8 W, the output spectrum with the fiber oscillator pumping is significantly broader than that with the ASE source pumping. For example, the simulated FWHM linewidth and 10-dB linewidth with the fiber oscillator pumping are 0.56 and 1.48 nm, respectively, while with the ASE source pumping, the corresponding spectral linewidths decrease to 0.44 and 1.02 nm. The spectral broadening is attributed to the self-phase modulation (SPM) effect [6,48]. Moreover, we have verified that the cross-phase modulation (XPM) between the pump wave and the 1st-order Stokes wave can be neglected. As the nonlinear length is much longer than the walk-off length, the XPM effect has no contribution to the spectral broadening [41].

Two factors lead to the difference in spectral broadening. One is the action length of the SPM effect; the other is the peak power (or the temporal fluctuation amplitude). As shown in Fig. 5(b), because of the higher effective Raman gain coefficient caused by strong pump intensity fluctuations, the 1st-order Stokes wave with the fiber oscillator pumping grows faster. Therefore, the action length of the SPM effect is much

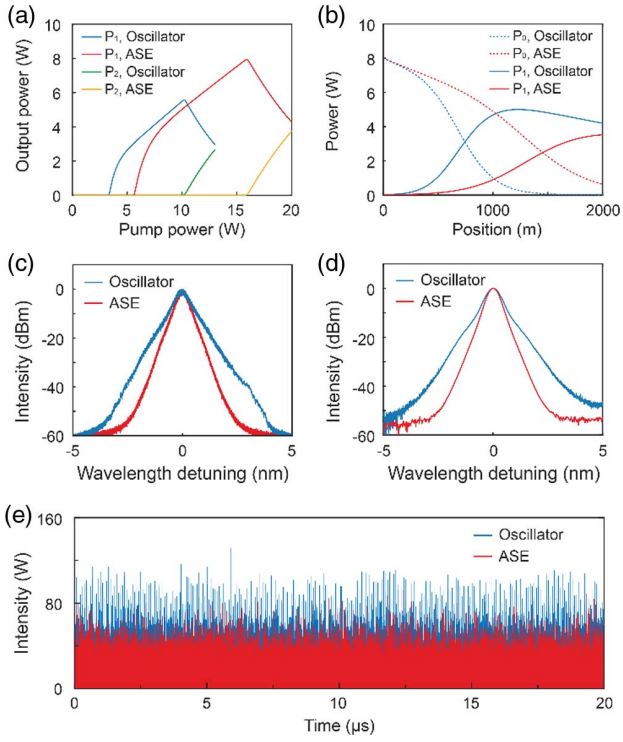

Fig. 5. Comparison of the output characteristics with the pumping of fiber oscillator and ASE source. (a) Simulated power evolutions and (b) longitudinal power distributions. (c) Simulated and (d) experimental output spectrum of the 1st-order Stokes wave. The central wavelength is 1120 nm. (e) Simulated temporal profiles of the 1st-order Stokes wave. The pump power for (b)–(e) is fixed at 8 W.

longer than that with ASE source pumping. Besides, the strong pump intensity fluctuations of the fiber oscillator can be transmitted to the RRFL, such as the self-mode locking with a repetition rate of ~13.2 MHz [shown in Fig. 1(c)]. Thus, the high peak powers can also be transferred from the pump source to the RRFL, which could enhance the SPM effect as well as the spectral broadening. Figure 5(e) shows the simulated temporal behaviors of the 1st-order Stokes wave at the output, which proves that the fiber oscillator-pumped RRFL has stronger temporal fluctuations than the ASE source-pumped counterpart. In addition, the simulated temporal profiles vary dramatically with the experimental results [see Fig. 3(b)]; this difference may be attributed to the limited bandwidths of the device and equipment used in the temporal measurement [49].

5. DISCUSSION

The pump fluctuation transfer in RRFLs differs greatly from that in rare-earth-doped random fiber lasers, and previous reports have confirmed that the fluctuations of pump sources are not correlated to that of the rare-earth-doped random fiber lasers [7]. In our opinion, the gain mechanism should be responsible for the difference. In RRFLs, the pump wave can directly interact with the random lasing through the SRS effect; thus, the pump intensity fluctuations can be transmitted to the generated random lasing. As the Raman response function shows a vibrational structure in the order of 100 fs, for a temporal fluctuation >1 ps, the SRS can be regarded as an instantaneous process [50]; while in rare-earth-doped random fiber lasers, the pump wave interacts with the active ions and affects the population inversion. As we know, the lifetime of the laser upper level is in the scale of milliseconds; thus, the fast fluctuations of the pump intensity could barely be transmitted to the population inversion. Or in other words, the pump intensity can be regarded as a constant in the temporal resolution of milliseconds. Therefore, the statistical properties of the rare-earth-doped random fiber lasers are related only to their operating status (e.g., below the threshold, near the threshold, and well above the threshold), instead of being correlated to the fluctuations of pump sources.

Here we would like to discuss further the impact of the pump intensity fluctuations on the output characteristics of the RRFL. As we know, the temporal fluctuations of the pump source could be transmitted to the RRFLs through the SRS process. On the one hand, the strong pump intensity fluctuations will increase the effective Raman gain coefficient, further influencing the longitudinal power distributions and the output power evolutions. On the other hand, the strong pump intensity fluctuations will affect the temporal behaviors of the generated random lasing, resulting in high fluctuation amplitude and high peak powers. Fortunately, the transfer of the pump intensity fluctuations is not an all-pass transmission in the frequency domain. Instead, a low-pass filtering effect exists due to the temporal walk-off effect between the pump wave and the random lasing.

Furthermore, the longitudinal power distributions and the temporal fluctuations of the random lasing will affect its own spectral broadening through the SPM effect. Thus, the fiber-oscillator-pumped RRFL shows a more pronounced spectral broadening. Additionally, we must point out that we have neglected the XPM effect here, since the nonlinear length is much longer than the walk-off length in our case. However, if the walk-off effect becomes weak or the operating power increases to a certain level, the nonlinear length would be comparable to the walk-off length; then the XPM would contribute to the spectral broadening.

Regulating the transfer of pump intensity fluctuations in RRFLs is critical to sensing, telecommunication, and high-power applications. For example, the sensing and telecommunication applications usually require light sources with a high spectral OSNR and superior RIN property. Employing a temporally stable pump source (such as the ASE source) or enhancing the walk-off effect may help realize high-performance RRFLs. On the one hand, employing a temporally stable pump source can suppress the transfer of temporal fluctuations from the root; on the other hand, enhancing the walk-off effect can narrow the frequency range of the intensity fluctuation transfer. The most straightforward way to enhance the walk-off effect is to increase the walk-off parameter, for example, using a high dispersion fiber or increasing the wavelength interval between the pump source and generated random lasing. Another way to enhance the walk-off effect is increasing the fiber length. However, this method plays a limited role, since the effective length is determined by the attenuation coefficient in very long fibers. For example, the commonly used SMF-28 fiber has an

effective length of ~20 km in the 1.5 μm range [2]; thus, the corresponding cut-off frequency is estimated to be ~30 MHz. In our experiment, the fiber oscillator shows a fundamental characteristic frequency of 13.2 MHz, which is within the cut-off frequency range, so the temporal fluctuations (such as the self-mode locking pulses) can be transferred from the fiber oscillator to the RRFLs. Therefore, a temporally stable pump source can benefit the ultralong RRFLs. In addition, the high-power RRFLs require short cavities to suppress the high-order SRS effect; increasing the fiber length seems not practical. Therefore, using a temporally stable pump source is particularly important in that case.

6. CONCLUSION

In summary, we experimentally and numerically investigated how the transfer of the pump intensity fluctuations influences the spectral, temporal, and power characteristics of an RRFL. For the power characteristic, strong pump intensity fluctuations could increase the effective Raman gain coefficient and result in the early onset of the 1st- and 2nd-order Stokes waves, further decreasing the maximum power of the 1st-order random lasing. For the spectral characteristic, strong pump intensity fluctuations could lead to more residual pump power, further limiting the improvement of maximum spectral purity and the OSNR. Particularly, we found that the stronger spectral broadening with fiber oscillator pumping can be attributed to the enhanced SPM effect, while the broad longitudinal power distribution and high peak powers of the 1st-order Stokes wave are responsible for enhancing the SPM effect. For the temporal characteristic, strong pump intensity fluctuations can be transmitted to the generated random lasing and result in an unstable temporal behavior. Fortunately, due to the temporal walk-off effect between the pump wave and the random lasing, there exists a low-pass filtering effect on the intensity fluctuation transfer. Moreover, we can regulate the walk-off effect (and the frequency range of intensity fluctuation transfer) through fiber dispersion and fiber length.

Owing to the transfer of pump intensity fluctuations and the influence of the temporal walk-off effect, the temporally stable ASE source-pumped RRFL shows ~45.3% higher maximum output power, higher spectral purity (>99.9%) and OSNR (>40 dB), weaker spectral broadening, and more stable temporal behavior compared to the temporally unstable fiber oscillator-pumped RRFL. We believe this work can help understand the impact of pump intensity fluctuations on the output characteristics of RRFLs, provide a reference for designing and implementing high-performance RRFLs, and promote their practicability in sensing, telecommunications, and high-power applications.

Funding. Hunan Provincial Innovation Construct Project (2019RS3018); National Natural Science Foundation of China (61905284, 62061136013).

Disclosures. The authors declare no conflicts of interest.

Data Availability. Data underlying the results presented in this paper are not publicly available at this time but may be obtained from the authors upon reasonable request.

REFERENCES

1. S. K. Turitsyn, S. A. Babin, A. E. El-Taher, P. Harper, D. V. Churkin, S. I. Kablukov, J. D. Ania-Castañón, V. Karalekas, and E. V. Podivilov, "Random distributed feedback fibre laser," Nat. Photonics **4**, 231–235 (2010).
2. S. K. Turitsyn, S. A. Babin, D. V. Churkin, I. D. Vatnik, M. Nikulin, and E. V. Podivilov, "Random distributed feedback fibre lasers," Phys. Rep. **542**, 133–193 (2014).
3. V. R. Supradeepa, Y. Feng, and J. W. Nicholson, "Raman fiber lasers," J. Opt. **19**, 023001 (2017).
4. S. A. Babin, "High-brightness all-fiber Raman lasers directly pumped by multimode laser diodes," High Power Laser Sci. Eng. **7**, e15 (2019).
5. D. V. Churkin, S. A. Babin, A. E. El-Taher, P. Harper, S. I. Kablukov, V. Karalekas, J. D. Ania-Castañón, E. V. Podivilov, and S. K. Turitsyn, "Raman fiber lasers with a random distributed feedback based on Rayleigh scattering," Phys. Rev. A **82**, 033828 (2010).
6. S. V. Smirnov and D. V. Churkin, "Modeling of spectral and statistical properties of a random distributed feedback fiber laser," Opt. Express **21**, 21236–21241 (2013).
7. B. C. Lima, A. S. L. Gomes, P. I. R. Pincheira, A. L. Moura, M. Gagné, E. P. Raposo, C. B. de Araújo, and R. Kashyap, "Observation of Lévy statistics in one-dimensional erbium-based random fiber laser," J. Opt. Soc. Am. B **34**, 293–299 (2017).
8. H. Wu, B. Han, Z. Wang, and H. Liang, "Statistical properties of Er/Yb co-doped random Rayleigh feedback fiber laser," Chin. Opt. Lett. **19**, 021402 (2021).
9. J. Deng, D. V. Churkin, Z. Xu, and X. Shu, "Random fiber laser based on a partial-reflection random fiber grating for high temperature sensing," Opt. Lett. **46**, 957–960 (2021).
10. S. Miao, W. Zhang, W. Huang, and Y. Song, "High-resolution static strain sensor based on random fiber laser and beat frequency interrogation," IEEE Photon. Technol. Lett. **31**, 1530–1533 (2019).
11. J. Xu, L. Huang, M. Jiang, J. Ye, P. Ma, J. Leng, J. Wu, H. Zhang, and P. Zhou, "Near-diffraction-limited linearly polarized narrow-linewidth random fiber laser with record kilowatt output," Photon. Res. **5**, 350–354 (2017).
12. A. S. L. Gomes, A. L. Moura, C. B. de Araújo, and E. P. Raposo, "Recent advances and applications of random lasers and random fiber lasers," Prog. Quant. Electron. **78**, 100343 (2021).
13. D. V. Churkin, S. Sugavanam, I. D. Vatnik, Z. Wang, E. V. Podivilov, S. A. Babin, Y. Rao, and S. K. Turitsyn, "Recent advances in fundamentals and applications of random fiber lasers," Adv. Opt. Photon. **7**, 516–569 (2015).
14. Z. Wang, H. Wu, M. Fan, L. Zhang, Y. Rao, W. Zhang, and X. Jia, "High power random fiber laser with short cavity length: theoretical and experimental investigations," IEEE J. Sel. Top. Quantum Electron. **21**, 0900506 (2015).
15. H. Zhang, L. Huang, P. Zhou, X. Wang, J. Xu, and X. Xu, "More than 400 W random fiber laser with excellent beam quality," Opt. Lett. **42**, 3347–3350 (2017).
16. H. Zhang, L. Huang, J. Song, H. Wu, P. Zhou, X. Wang, J. Wu, J. Xu, Z. Wang, X. Xu, and Y. Rao, "Quasi-kilowatt random fiber laser," Opt. Lett. **44**, 2613–2616 (2019).
17. I. A. Lobach, S. I. Kablukov, and S. A. Babin, "Linearly polarized cascaded Raman fiber laser with random distributed feedback operating beyond 1.5 μm," Opt. Lett. **42**, 3526–3529 (2017).
18. J. Ye, Y. Zhang, J. Xu, J. Song, T. Yao, H. Xiao, J. Leng, and P. Zhou, "Investigations on the extreme frequency shift of phosphosilicate random fiber laser," J. Lightwave Technol. **38**, 3737–3744 (2020).
19. Z. Wang, M. Fan, H. Wu, Y. Li, Y. Li, L. Zhang, and Y. Rao, "Cascaded random distributed-feedback Raman fiber laser assisted by Fresnel reflection," Opt. Express **23**, 28076–28081 (2015).
20. S. A. Babin, A. E. El-Taher, P. Harper, E. V. Podivilov, and S. K. Turitsyn, "Tunable random fiber laser," Phys. Rev. A **84**, 021805 (2011).
21. J. Nuño, M. Alcon-Camas, and J. D. Ania-Castañón, "RIN transfer in random distributed feedback fiber lasers," Opt. Express **20**, 27376–27381 (2012).
22. J. Xu, Z. Lou, J. Ye, J. Wu, J. Leng, H. Xiao, H. Zhang, and P. Zhou, "Incoherently pumped high-power linearly-polarized single-mode

random fiber laser: experimental investigations and theoretical prospects," Opt. Express **25**, 5609–5617 (2017).
23. L. Zhang, J. Dong, and Y. Feng, "High-power and high-order random Raman fiber lasers," IEEE J. Sel. Top. Quantum Electron. **24**, 1400106 (2018).
24. J. Dong, L. Zhang, H. Jiang, X. Yang, W. Pan, S. Cui, X. Gu, and Y. Feng, "High order cascaded Raman random fiber laser with high spectral purity," Opt. Express **26**, 5275–5280 (2018).
25. V. Balaswamy, S. Ramachandran, and V. R. Supradeepa, "High-power, cascaded random Raman fiber laser with near complete conversion over wide wavelength and power tuning," Opt. Express **27**, 9725–9732 (2019).
26. J. Ye, J. Xu, J. Song, Y. Zhang, H. Zhang, H. Xiao, J. Leng, and P. Zhou, "Pump scheme optimization of an incoherently pumped high-power random fiber laser," Photon. Res. **7**, 977–983 (2019).
27. Y. Zhang, J. Song, J. Ye, J. Xu, T. Yao, and P. Zhou, "Tunable random Raman fiber laser at 1.7 μm region with high spectral purity," Opt. Express **27**, 28800–28807 (2019).
28. J. Ye, C. Fan, J. Xu, H. Xiao, J. Leng, and P. Zhou, "2-kW-level superfluorescent fiber source with flexible wavelength and linewidth tunable characteristics," High Power Laser Sci. Eng. **9**, e55 (2021).
29. J. Song, H. Wu, J. Ye, J. Xu, H. Zhang, and P. Zhou, "High power linearly polarized Raman fiber laser with stable temporal output," Photon. Sens. **9**, 43–48 (2019).
30. Y. Chen, J. Song, J. Ye, T. Yao, J. Xu, H. Xiao, J. Leng, and P. Zhou, "Power scaling of Raman fiber amplifier based on the optimization of temporal and spectral characteristics," Opt. Express **28**, 12395–12404 (2020).
31. X. Cheng, S. Cui, X. Zeng, J. Zhou, and Y. Feng, "Spectral and RIN properties of a single-frequency Raman fiber amplifier co-pumped by ASE source," Opt. Express **29**, 15764–15771 (2021).
32. K. Hammani, C. Finot, J. M. Dudley, and G. Millot, "Optical rogue-wave-like extreme value fluctuations in fiber Raman amplifiers," Opt. Express **16**, 16467–16474 (2008).
33. K. Hammani, A. Picozzi, and C. Finot, "Extreme statistics in Raman fiber amplifiers: from analytical description to experiments," Opt. Commun. **284**, 2594–2603 (2011).
34. E. J. R. Kelleher, J. C. Travers, S. V. Popov, and J. R. Taylor, "Role of pump coherence in the evolution of continuous-wave supercontinuum generation initiated by modulation instability," J. Opt. Soc. Am. B **29**, 502–511 (2012).
35. E. J. R. Kelleher, "Pump wave coherence, modulation instability and their effect on continuous-wave supercontinua," Opt. Fiber Technol. **18**, 268–282 (2012).
36. F. Brunet, Y. Taillon, P. Galarneau, and S. LaRochelle, "A simple model describing both self-mode locking and sustained self-pulsing in ytterbium-doped ring fiber lasers," J. Lightwave Technol. **23**, 2131–2138 (2005).
37. J. Xu, J. Wu, J. Ye, J. Song, B. Yao, H. Zhang, J. Leng, W. Zhang, P. Zhou, and Y. Rao, "Optical rogue wave in random fiber laser," Photon. Res. **8**, 1–7 (2020).
38. H. Zhang, H. Xiao, P. Zhou, X. Wang, and X. Xu, "Random distributed feedback Raman fiber laser with short cavity and its temporal properties," IEEE Photon. Technol. Lett. **26**, 1605–1608 (2014).
39. W. Liu, P. Ma, Y. Miao, H. Wu, P. Zhou, and Z. Jiang, "Intrinsic mechanism for spectral evolution in single-frequency Raman fiber amplifier," IEEE J. Sel. Top. Quantum Electron. **24**, 3100408 (2018).
40. S. Rota-Rodrigo, G. Rizzelli, D. Leandro, J. Nuño, M. Lopez-Amo, G. Santarelli, and J. D. Ania-Castañón, "Anomalous relative intensity noise transfer in ultralong random fiber lasers," Opt. Express **28**, 28234–28242 (2020).
41. D. V. Churkin, O. A. Gorbunov, and S. V. Smirnov, "Extreme value statistics in Raman fiber lasers," Opt. Lett. **36**, 3617–3619 (2011).
42. S. K. Turitsyn, A. E. Bednyakova, M. P. Fedoruk, A. I. Latkin, A. A. Fotiadi, A. S. Kurkov, and E. Sholokhov, "Modeling of CW Yb-doped fiber lasers with highly nonlinear cavity dynamics," Opt. Express **19**, 8394–8405 (2011).
43. D. V. Churkin, S. V. Smirnov, and E. V. Podivilov, "Statistical properties of partially coherent cw fiber lasers," Opt. Lett. **35**, 3288–3290 (2010).
44. P. Suret, R. E. Koussaifi, A. Tikan, C. Evain, S. Randoux, C. Szwaj, and S. Bielawski, "Single-shot observation of optical rogue waves in integrable turbulence using time microscopy," Nat. Commun. **7**, 13136 (2016).
45. W. Liu, P. Ma, P. Zhou, Z. Jiang, H. Ackermann, W. L. Bohn, and D. H. Titterton, "Optimization for the fiber laser source through its temporal and spectral characteristics," Proc. SPIE **10436**, 104360O (2017).
46. F. Vanholsbeeck, S. Martin-Lopez, M. Gonzalez-Herraez, and S. Coen, "The role of pump incoherence in continuous-wave supercontinuum generation," Opt. Express **13**, 6615–6625 (2005).
47. J. Ye, X. Ma, Y. Zhang, J. Xu, H. Zhang, T. Yao, J. Leng, and P. Zhou, "From spectral broadening to recompression: dynamics of incoherent optical waves propagating in the fiber," PhotoniX **2**, 15 (2021).
48. S. A. Babin, E. A. Zlobina, S. I. Kablukov, and E. V. Podivilov, "High-order random Raman lasing in a PM fiber with ultimate efficiency and narrow bandwidth," Sci. Rep. **6**, 22625 (2016).
49. O. A. Gorbunov, S. Sugavanam, and D. V. Churkin, "Revealing statistical properties of quasi-CW fibre lasers in bandwidth-limited measurements," Opt. Express **22**, 28071–28076 (2014).
50. G. P. Agrawal, *Nonlinear Fiber Optics* (Academic, 2013).